


## PAPER

[View Article Online](#)  
[View Journal](#) | [View Issue](#)Cite this: *J. Mater. Chem. A*, 2023, **11**, 1232

## Atmospheric humidity-triggered reversible spin-state switching†

Yang-Hui Luo, \* Hui Dong, Shu-Hua Ma, Feng-Lian Zeng, Xue-Ting Jin and Min Liu

The practical application of molecular switches is highly dependent on the reversible spin-state switching under ambient conditions, which needs a delicate materials design. Here, by confining a spin-crossover material into a sponge, the challenging goal of reversible spin-state switching in the solid state under ambient conditions has been realized, upon irradiation with a 980 nm laser for 120 s followed by shutting off the laser for 150 s. More importantly, further integration of the hygroscopic material has endowed the sponge with the merits of effective atmospheric humidity-triggered reversible spin-state switching under ambient conditions for the first time, accompanied by a reversible color variation upon naturally occurring humidity capture/release cycles. This work is expected to provide a fairly good strategy for developing novel molecular switches triggered by natural energy sources at the device level.

Received 4th November 2022  
Accepted 5th December 2022

DOI: 10.1039/d2ta08632h

[rsc.li/materials-a](https://rsc.li/materials-a)

## Introduction

Switchable magnetization, or the so-called spin-crossover (SCO), refers to the re-arrangement of spin sites between high-spin (HS) and low-spin (LS) states as a response to external stimuli.<sup>1–6</sup> This kind of spin-state switching is usually accompanied by reversible variations in magnetic, mechanical, dielectric, and optical properties, thus showing the potential to be applied in molecular memory, sensors, displays, molecular electronics, *etc.*<sup>6–10</sup> Among these external stimuli, photo-irradiation has shown the most-practical value, owing to the merits of high local precision, high polarization, remote controllability, temporal dynamics, and ease of manipulation.<sup>11–16</sup> The typical examples of photo-triggered spin-state switching are the light-induced excited spin-state trapping (LIESST) and reverse LIESST, which involve visible-light-induced LS-to-HS state transition and near-infrared (NIR) light-induced HS-to-LS state transition, respectively, giving rise to practical application in photo-triggered memory devices.<sup>17–20</sup> However, both the LIESST and reverse LIESST usually occurred below 100 K, which limited greatly their wide application. Hence, the design of a special system with photo-triggered spin-state switching under ambient conditions is of significant importance.

The search for external stimuli from the ambient environment to trigger spin-state switching has shown promising potential for practical applications, as it can promote the challenging goal of “energy conservation and emission

reduction”.<sup>21–23</sup> Among the various energy sources in the ambient environment, atmospheric humidity is rather overlooked owing to its annoying attributes.<sup>24–26</sup> However, the earth's atmospheric humidity was estimated to be about 13 000 trillion liters, and the conversion of this huge free source to use physical forms, electrical energies, and physical signals, will certainly make a big difference in the development of a sustainable society.<sup>27–30</sup> From this point of view, the use of atmospheric humidity to trigger spin-state switching, which remains un-studied, represents an effective strategy for “energy conservation and emission reduction”, and is expected to promote the device application of atmospheric humidity-related detection, displays, and switching.

Here in this work, *via* confinement of a two-dimensional (2D) SCO material into a hygroscopic sponge, the atmospheric humidity-triggered reversible spin-state switching under ambient conditions has been achieved. The related sponge was composed of a hydrophobic polymer poly(vinylidene fluoride) (PVDF) and a hydrophilic polymer polyethylene glycol (PEG),<sup>31</sup> which act as a three-dimensional bracket that disperses the 2D SCO material in space. The related 2D SCO material was an NIR-sensitive species 2D-SCO@UCNPs (Fig. 1),<sup>32</sup> where, 2D-SCO = single-layered 2D nanosheets of the SCO material [Fe(1,3-bis(4-pyridyl)-propane)<sub>2</sub>(SCN)<sub>2</sub>]<sub>2</sub>;<sup>33</sup> and UCNPs = zero-dimensional (0D) upconverting nanoparticles NaYF<sub>4</sub>:20 mol% Yb<sup>3+</sup>, 1 mol% Er<sup>3+</sup>, which are capable of upconverting 980 nm NIR-light into 500–700 nm visible-light that matches well with the energy required for spin-state switching of 2D-SCO.<sup>34</sup> Upon photo-irradiation with a 980 nm laser, the species of 2D-SCO@UCNPs in the sponge has shown a complete HS-to-LS transition, which was reverse LIESST, within 120 s, and shutting off the laser can induce the reverse LS-to-HS transition within 150 s, suggesting a photo-triggered reversible spin-state

School of Chemistry and Chemical Engineering, Southeast University, Nanjing, 211189, P. R. China. E-mail: [luoyh2016@seu.edu.cn](mailto:luoyh2016@seu.edu.cn)

† Electronic supplementary information (ESI) available. See DOI: <https://doi.org/10.1039/d2ta08632h>



Fig. 1 Schematics of the fabrication process and materials used for the sponges; the photo- and humidity-triggered reversible spin-state switching under ambient conditions have been highlighted.

switching in the solid state under ambient conditions. More importantly, in the presence of the hygroscopic material,<sup>35</sup> atmospheric humidity-triggered reversible spin-state switching under ambient conditions, accompanied by a dramatic reversible color variation of the sponge, has been observed, which was due to the naturally occurring humidity capture/release cycles within the hygroscopic sponge (Fig. 1). At this point, the challenging goal of “energy conservation” has been realized with the hygroscopic sponge. Being an effective way to develop the natural energy source-triggered molecular switching at the device level, the present work may open a new avenue for the development of next-generation molecular switch systems.

## Results and discussion

### Fabrication of the sponge

The fabrication process and materials used for the sponge are illustrated in Fig. 1. 2D-SCO, UCNPs, 2D-SCO@UCNPs, and the naked sponge were prepared according to our previous work,<sup>31–36</sup> their transmission electron microscopy (TEM) images are presented at the bottom of Fig. 1. The obtained naked sponge was almost colorless (Fig. S1†), while after being incorporated with yellow-colored 2D-SCO@UCNPs, the sponge displayed a uniformly distributed bright yellow color (Fig. 2a), suggesting the fine dispersion of 2D-SCO@UCNPs in the sponge. Interestingly, this kind of sponge is porous (Fig. 2b), which can act as a channel for the transmission of small molecules.<sup>31</sup> IR spectra have suggested that the confinement in the sponge has made a significant influence on the intermolecular interactions of 2D-SCO@UCNPs, as the vibrational peaks for SCN (at around  $2000\text{ cm}^{-1}$ ) have decreased dramatically in the sponge (Fig. 2c).

For comparison, confining of individual 2D-SCO into the sponge has been performed. As expected, a similar bright-yellow color for 2D-SCO in the sponge has been observed (Fig. S2†), which is also accompanied by a dramatic decrease of the vibrational peaks for SCN (at around  $2000\text{ cm}^{-1}$ ) (Fig. 2d). From this point of view, the electronic state around the Fe(II) ion in 2D-SCO@UCNPs must have been altered after being confined in the sponge, and at this point, the effective spin-state switching can be expected in the sponge state.

### NIR-triggered spin-state switching

Fig. 3a shows that the confinement in the sponge has improved three times the intensity of the metal-to-ligand charge transfer (MLCT) bands for 2D-SCO (550–700 nm), which matches well with the energy of the green up-converting light (UCL) from the UCNPs irradiated with a 980 nm laser.<sup>36–38</sup> These results have demonstrated significantly the superiority of the sponge for photo-triggered spin-state switching. Note that, compared with 2D-SCO in the sponge, a further increase of the MLCT bands has been observed for 2D-SCO@UCNPs in the sponge, which was accompanied by a decrease of the d–d transition bands (at around 480 nm) for the LS state Fe(II) species (Fig. 3b), suggesting that UCNPs will play a key role for the photo-triggered spin-state switching in the sponge. More interestingly, compared with individual 2D-SCO@UCNPs which shows mainly the LS state Fe(II) species (Fig. 3b), the confinement in the sponge has induced the HS state. In this sense, promising photo-triggered spin-state switching in the sponge under ambient conditions is certain.

We then irradiated 2D-SCO@UCNPs in the sponge with a 980 nm laser under ambient conditions, and as expected, a remarkable decrease of the MLCT bands (centered at 625 nm),

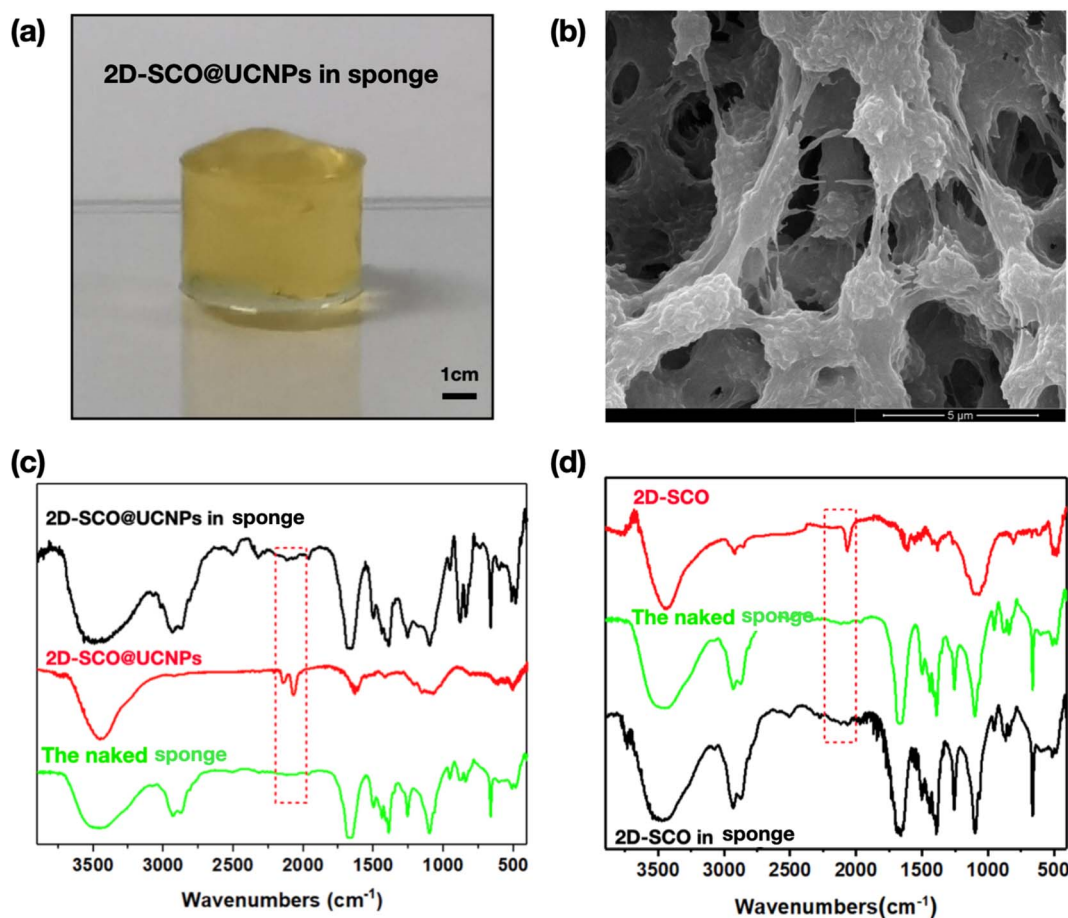


Fig. 2 (a) Optical and (b) SEM images of 2D-SCO@UCNPs in the sponge; IR spectra illustrating the variation of intermolecular interactions for (c) 2D-SCO@UCNPs and (d) 2D-SCO in the sponge.

as well as a remarkable increase of the d–d(Fe) transition bands for the LS state (centered at 480 nm), have been observed with irradiation for only 30 s (Fig. 3c), which corresponded to the photo-triggered reverse LIESST. Note that, these variations can be further strengthened until 120 s, suggesting that the complete HS to LS state transition has been completed in the sponge within 120 s. Importantly, the reverse process, that is the complete LS to HS state transition, can be achieved by shutting off the laser for 150 s, demonstrating that for the first time, the challenging goal of photo-triggered reversible spin-state switching under ambient conditions, has been achieved in the sponge state with alternating NIR laser on for 120 s followed by laser off for 150 s. More interestingly, the above-mentioned reversible process is expected to be repeated infinitely, with no decrease in the efficiency that can be observed after 5 cycles (Fig. 3d), suggesting that the present sponge has shown potential to be practically applied as a switching device.

For practical applications, excellent stability and chemical tolerance are the premises. The porous features have suggested that the sponge may undergo shrinkage and swelling. To verify this aspect, heating of the sponges (including the naked sponge, 2D-SCO in the sponge, and 2D-SCO@UCNPs in the sponge) under 45 °C has been performed, as shown in Fig. S3†; upon heating, all the sponges had undergone continuous shrinking

and color-darkening, reaching about one-fourth of the original volume within 30 min. Interestingly, Raman spectra that track the heating process have suggested that the shrunk sponges, for both the “2D-SCO in the sponge” (Fig. S4†) and “2D-SCO@UCNPs in the sponge” (Fig. S5†), all have shown identical spectra with the shrunk naked sponge (Fig. S6†). More importantly, these heated sponges can be restored to their initial state by being immersed in a DMF solution. As shown in Fig. S7 and S8,† the shrunk sponges have undergone continuous swelling upon DMF immersion, reaching 75% of the initial volume within 30 min, suggesting vividly the reversible shrinking-swelling performance. Meanwhile, this reversible shrinking-swelling did not destroy the integrity of the sponge, as the recovered species have shown almost identical Raman spectra with the initial samples (Fig. S4–S6†). In this sense, the excellent stability and chemical tolerance of the present sponge are expected to promote its practical application in complex environments.

#### Atmospheric humidity-triggered spin-state switching

Considering that the porous features can promote small molecules, such as water, through the sponge, we then focus on the practical application of the sponge in a humid environment, to achieve the ambition of “energy conservation”, that is,



Fig. 3 (a) UV-vis absorption spectra of 2D-SCO, 2D-SCO in the sponge, and the UCL emission of UCNP, and the inset shows the photograph of green emission from the UCNP in a hexane solution excited with a 980 nm laser; (b) comparison between the UV-vis absorption of 2D-SCO@UCNPs, 2D-SCO in the sponge and 2D-SCO@UCNPs in the sponge; (c) time-dependent variation of UV-vis absorption spectra for 2D-SCO@UCNPs in the sponge under irradiation with a 980 nm laser; (d) alternating laser on and off as a function of the absorption intensity in (c) at 625 nm.

atmospheric humidity-triggered spin-state switching. For this purpose, the 2D super hygroscopic material,<sup>31,35</sup> which featured efficient humidity capture capacity under ambient conditions, as well as fast water release triggered by natural sunlight, has been employed. As shown in Fig. 4a, the integration of the blue-colored super hygroscopic material into the yellow-colored sponge has given birth to a blackish-green-colored hygroscopic sponge. Under an atmosphere with a relative humidity of 90% at room temperature, this hygroscopic sponge can capture humidity rapidly, accompanied by a dramatic color change from blackish-green (humidity content of 0%), through the intermediate state green (humidity content of 13%), to finally yellow (humidity content of 25%). Note that, this color variation can be attributed to the different intermolecular interactions involving the water molecules and 2D surfaces of both hygroscopic and SCO materials.<sup>39–44</sup> Importantly, this color-variation process is reversible, as the yellow-colored species (humidity content of 25%) can return to the blackish-green state, upon humidity release triggered by natural sunlight, which also goes through an intermediate state of green (humidity content of 12%, Fig. 4a). These results have demonstrated significantly the practical potential of this hygroscopic sponge for humidity-related sensing, display, response, monitoring, and so on.

To further demonstrate the above-mentioned promising aspect, the humidity content-dependent UV-vis absorption

spectra of the hygroscopic sponge have been collected. Fig. 4b shows that upon humidity capture, the MLCT bands (centered at 625 nm) of 2D-SCO@UCNPs have undergone a continuous increase with humidity contents increasing from 0 to 25% (water capture  $\text{g g}^{-1}$  of the sponge), corresponding to the LS-to-HS transition. While upon humidity release with humidity content decrease from 25 to 2%, the increased MLCT bands fall back (Fig. 4c), suggesting the reverse HS-to-LS transition. At this time, atmospheric humidity-triggered reversible spin-state switching has been demonstrated for the first time. One thing that should be stressed is that this kind of HS-to-LS transition is not exactly the reverse process of the LS-to-HS transition, as the humidity release process was much slower than the humidity capture process, giving birth to a hysteresis loop for larger than 10% humidity content on the  $\gamma_{\text{HS}}$  vs. humidity content plots (Fig. 4d). This phenomenon can be attributed to the strong interactions between the water molecules and the 2D surfaces of the SCO material, making it difficult for water release. More important, for the yellow-colored hygroscopic sponge (the hygroscopic sponge with a humidity content of 25%), photo-triggered reverse LIESST, which was the HS-to-LS transition, can also be observed within 120 s (Fig. 4e), suggesting that the presence of water molecules does not affect the spin-state transition performance of 2D-SCO@UCNPs in the hygroscopic sponge. Hence, for the first time, the atmospheric humidity-





Fig. 4 (a) Photo images showing the fabrication process of the hygroscopic sponge, and the color-variation as a response to humidity capture/release; (b) variation of UV-vis absorption spectra of the hygroscopic sponge with the humidity content increase from 0 to 25% and (c) decrease from 25 to 2%  $\text{g g}^{-1}$  of the sponge; (d) the related  $\gamma_{HS}$  vs. humidity content plots; (e) photo-triggered reverse LIESST of the hygroscopic sponge with a humidity content of 25%.

triggered spin-state transition, which occurred naturally under ambient conditions in the sponge state, has been realized.

## Conclusion

In summary, we have demonstrated that *via* the confinement in the sponge, the 2D SCO material 2D-SCO@UCNPs can show effective photo-triggered reversible spin-state switching with alternating laser on and laser off under ambient conditions. Furthermore, with the incorporation of the hygroscopic material, the hygroscopic sponge has shown atmospheric humidity-triggered reversible spin-state switching and color variation for the first time, as a response to naturally occurring humidity capture/release cycles, achieving the challenging goal of “energy conservation” at the device level. Given the vigorous

developments in SCO materials with multiple functions, our work provides a fairly good prototype for the development of multi-functional molecular switching triggered by natural energy sources in the ambient environment.

## Experimental section

### General considerations

All syntheses were performed under ambient conditions and all the chemicals were of analytical grade and were used without further purification.

### Characterization

The surface morphologies of the sponge were characterized using a field emission scanning electron microscope (FE-SEM),

HITACHI S-4800 20 kV). Infrared spectra were recorded on a Shimadzu IR Prestige-21 FTIR-8400S spectrometer in the spectral range 4000–500  $\text{cm}^{-1}$ , with the samples in the form of potassium bromide pellets. UCL spectra of UCNPs were measured with a fluorescence spectrometer (Edinburgh, LFS-920) using an external CW 980 nm laser (Xi'an Saipulin Laser Technology Institute, China) with a tunable power of 0–3 W acting as the excitation source. UV-vis absorption spectra were recorded with a Shimadzu UV-3150 double-beam spectrophotometer. The irradiation experiments were performed by using a CW 980 nm NIR laser (SD980-5000G3, Xi'an Saipulin Laser Technology Institute, China) at a laser power density of 1.0 W  $\text{cm}^{-2}$ . Raman spectra were recorded using a Raman microscope (Kaiser Optical Systems, Inc., Ann Arbor, MI, USA) with 785 nm laser excitation, and the spectra were obtained by 2 min exposure of the CCD detector in the wavenumber range 50–3500  $\text{cm}^{-1}$ .

### Preparation of 2D-SCO@UCNPs

The preparation of 2D-SCO@UCNPs was reported in our previous work.<sup>35–38</sup>

### Preparation of the naked sponge

To a 50 mL three-necked flask with PEG-6000 (0.45 g), 15 mL of DMF was added, which was ultrasonicated for 10 min to completely dissolve. Then 2 g of PVDF was added slowly and the resulting mixtures were stirred for 3 h to get a clear solution. Products of the naked sponge were obtained by placing the solution in the mold for 24 h after degassing.

### Preparation of 2D-SCO@UCNPs in the sponge

To a 50 mL three-necked flask with PEG-6000 (0.45 g), 15 mL of DMF was added, which was ultrasonicated for 10 min to completely dissolve. Then 2 g of PVDF was added slowly and the resulting mixtures were stirred for 3 h to get a clear solution. After that, 36 mg of 2D-SCO@UCNPs was added and stirred for 1 h. The resulting suspension was then transferred to a 90 °C water bath with continuous stirring for 6 hours. Products of 2D-SCO@UCNPs in the sponge were obtained by placing the solution in the mold for 24 h after cooling to room temperature and degassing.

### Preparation of 2D-SCO in the sponge

To a 50 mL three-necked flask with PEG-6000 (0.45 g), 15 mL of DMF was added, which was ultrasonicated for 10 min to completely dissolve. Then 2 g of PVDF was added slowly, and the resulting mixtures were stirred for 3 h to get a clear solution. After that, 30 mg of 2D-SCO was added and stirred for 1 h. The resulting suspension was then transferred to a 90 °C water bath with continuous stirring for 6 hours. Products of 2D-SCO in the sponge were obtained by placing the solution in the mold for 24 h after cooling to room temperature and degassing.

### Preparation of the hygroscopic sponge

It is identical with the process for fabrication of 2D-SCO@UCNPs in the sponge, except for the addition of 5 mg of

the hygroscopic material. To a 50 mL three-necked flask with PEG-6000 (0.45 g), 15 mL of DMF was added, which was ultrasonicated for 10 min to completely dissolve. Then 2 g of PVDF was added slowly, and the resulting mixtures were stirred for 3 h to get a clear solution. After that, 5 mg of the hygroscopic material and 30 mg of 2D-SCO@UCNPs were added and stirred for 1 h. The resulting suspension was then transferred to a 90 °C water bath with continuous stirring for 6 hours. Products of the hygroscopic sponge were obtained by placing the solution in the mold for 24 h after cooling to room temperature and degassing.

### Humidity capture for the hygroscopic sponge

Under the atmosphere at a relative humidity of 90% (created by the saturated aqueous solution of KCl), the hygroscopic sponge was put on glass and exposed to the atmosphere. The adsorption rates and adsorption capacities were investigated by weighing the adsorbed species on an electronic balance at the set time interval. The variations in phase state were recorded using a camera.

### Humidity release for the hygroscopic sponge

The humidity release process was carried out by using a halogen lamp (AM 1.5) to irradiate the yellow-colored hygroscopic sponge, and the desorption rates were investigated by weighing the desorbed species on an electronic balance at the set time interval.

## Conflicts of interest

The authors declare no competing financial interest.

## Acknowledgements

This research was supported by the Jiangsu Provincial Department of Science and Technology Innovation Support Program (No. BZ2022036), the Natural Science Foundation of China, the Zhishan Youth Scholar Program of SEU, and the PAPD of Jiangsu Higher Education Institutions.

## References

- 1 L. Zhao, Y. S. Meng, Q. Liu, O. Sato, Q. Shi, H. Oshio and T. Liu, *Nat. Chem.*, 2021, **13**, 698–704.
- 2 V. Rubio-Gimenez, S. Tatay and C. Marti-Gastaldo, *Chem. Soc. Rev.*, 2020, **49**, 5601–5638.
- 3 R. Torres-Cavanillas, R. Sanchis-Gual, J. Dugay, M. Coronado-Puchau, M. Gimenez-Marques and E. Coronado, *Adv. Mater.*, 2019, **31**, e1900039.
- 4 Y. S. Meng and T. Liu, *Acc. Chem. Res.*, 2019, **52**, 1369–1379.
- 5 M. Palluel, N. M. Tran, N. Daro, S. Buffière, S. Mornet, E. Freysz and G. Chastanet, *Adv. Funct. Mater.*, 2020, **30**, 2000447.
- 6 T. Boonprab, S. J. Lee, S. G. Telfer, K. S. Murray, W. Phonsri, G. Chastanet, E. Collet, E. Trzop, G. N. L. Jameson, P. Harding and D. J. Harding, *Angew. Chem., Int. Ed.*, 2019, **58**, 11811–11815.

- 7 S. Liu, K. Zhou, T. Yuan, W. Lei, H. Y. Chen, X. Wang and W. Wang, *J. Am. Chem. Soc.*, 2020, **142**, 15852–15859.
- 8 K. Ridier, A. C. Bas, Y. Zhang, L. Routaboul, L. Salmon, G. Molnar, C. Bergaud and A. Bousseksou, *Nat. Commun.*, 2020, **11**, 3611.
- 9 J. Liu, Y. Gao, T. Wang, Q. Xue, M. Hua, Y. Wang, L. Huang and N. Lin, *ACS Nano*, 2020, **14**, 11283–11293.
- 10 M. Mikolasek, K. Ridier, D. Bessas, V. Cerantola, G. Felix, G. Chaboussant, M. Piedrahita-Bello, E. Angulo-Cervera, L. Godard, W. Nicolazzi, L. Salmon, G. Molnar and A. Bousseksou, *J. Phys. Chem. Lett.*, 2019, **10**, 1511–1515.
- 11 M. J. Heras Ojea, J. M. Van Raden, S. Louie, R. Collins, D. Pividori, J. Cirera, K. Meyer, R. Jasti and R. A. Layfield, *Angew. Chem., Int. Ed.*, 2021, **60**, 3515–3518.
- 12 J. Cruddas and B. J. Powell, *J. Am. Chem. Soc.*, 2019, **141**, 19790–19799.
- 13 A. Enriquez-Cabrera, A. Rapakousiou, M. Piedrahita Bello, G. Molnár, L. Salmon and A. Bousseksou, *Coord. Chem. Rev.*, 2020, **419**, 213396.
- 14 K. Senthil Kumar and M. Ruben, *Coord. Chem. Rev.*, 2017, **346**, 176–205.
- 15 V. B. Jakobsen, E. Trzop, L. C. Gavin, E. Dobbelaar, S. Chikara, X. Ding, K. Esien, H. Muller-Bunz, S. Felton, V. S. Zapf, E. Collet, M. A. Carpenter and G. G. Morgan, *Angew. Chem., Int. Ed.*, 2020, **59**, 13305–13312.
- 16 A. Kawamura, J. Xie, J. N. Boyn, K. A. Jesse, A. J. McNeece, E. A. Hill, K. A. Collins, J. A. Valdez-Moreira, A. S. Filatov, J. W. Kurutz, D. A. Mazziotti and J. S. Anderson, *J. Am. Chem. Soc.*, 2020, **142**, 17670–17680.
- 17 S. Decurtins, P. Gütlisch, C. P. Kohler, H. Spiering and A. Hauser, *Chem. Phys. Lett.*, 1984, **105**, 1–4.
- 18 J.-F. Letard, P. Guionneau, L. Rabardel, J. A. K. Howard, A. E. Goeta, D. Chasseau and O. Kahn, *Inorg. Chem.*, 1998, **37**, 4432–4441.
- 19 S. Hayami, Z. Gu, M. Shiro, Y. Einaga, A. Fujishima and O. Sato, *J. Am. Chem. Soc.*, 2000, **122**, 7126–7127.
- 20 Y. Ogawa, S. Koshihara, K. Koshino, T. Ogawa, C. Urano and H. Takagi, *Phys. Rev. Lett.*, 2000, **84**, 3181–3184.
- 21 H. Arazoe, D. Miyajima, K. Akaike, F. Araoka, E. Sato, T. Hikima, M. Kawamoto and T. Aida, *Nat. Mater.*, 2016, **15**, 1084–1089.
- 22 X. Chen, D. Goodnight, Z. Gao, A. H. Cavusoglu, N. Sabharwal, M. DeLay, A. Driks and O. Sahin, *Nat. Commun.*, 2015, **6**, 7346.
- 23 J. Chen, Y. Huang, N. N. Zhang, H. Y. Zou, R. Y. Liu, C. Y. Tao, X. Fan and Z. L. Wang, *Nat. Energy*, 2016, **1**, 16138.
- 24 M. Wang, T. Sun, D. Wan, M. Dai, S. Ling, J. Wang, Y. Liu, Y. Fang, S. Xu, J. Yeo, H. Yu, S. Liu, Q. Wang, J. Li, Y. Yang, Z. Fan and W. Chen, *Nano Energy*, 2021, **80**, 105569.
- 25 J. Yang, X. Zhang, H. Qu, Z. G. Yu, Y. Zhang, T. J. Eey, Y. W. Zhang and S. C. Tan, *Adv. Mater.*, 2020, **32**, e2002936.
- 26 F. Ni, N. Qiu, P. Xiao, C. Zhang, Y. Jian, Y. Liang, W. Xie, L. Yan and T. Chen, *Angew. Chem., Int. Ed.*, 2020, **59**, 19237–19246.
- 27 D. K. Nandakumar, Y. Zhang, S. K. Ravi, N. Guo, C. Zhang and S. C. Tan, *Adv. Mater.*, 2019, **31**, e1806730.
- 28 D. K. Nandakumar, S. K. Ravi, Y. Zhang, N. Guo, C. Zhang and S. C. Tan, *Energy Environ. Sci.*, 2018, **11**, 2179–2187.
- 29 F. Zhao, X. Zhou, Y. Liu, Y. Shi, Y. Dai and G. Yu, *Adv. Mater.*, 2019, **31**, e1806446.
- 30 L. Zhang, W.-X. Fang, C. Wang, H. Dong, S.-H. Ma and Y.-H. Luo, *Inorg. Chem. Front.*, 2021, **8**, 898–913.
- 31 C. Xue, S.-X. Zhang, F.-L. Zeng, H. Dong, S.-H. Ma and Y.-H. Luo, *Adv. Mater. Technol.*, 2022, DOI: [10.1002/admt.202201188](https://doi.org/10.1002/admt.202201188).
- 32 J.-Y. Wang, C. Chen, C. He, Z.-Y. Zheng, C. Wang, D.-L. Hong, X.-T. He, Y.-H. Luo and B.-W. Sun, *J. Mater. Chem. C*, 2019, **7**, 3965–3972.
- 33 Y. H. Luo, C. Chen, G. W. Lu, D. L. Hong, X. T. He, C. Wang, J. Y. Wang and B. W. Sun, *J. Phys. Chem. Lett.*, 2018, **9**, 7052–7058.
- 34 Y. H. Luo, J. W. Wang, W. Wang, X. T. He, D. L. Hong, C. Chen, T. Xu, Q. Shao and B. W. Sun, *ACS Appl. Mater. Interfaces*, 2018, **10**, 16666–16673.
- 35 Y.-H. Luo, C. Wang, S.-H. Ma, X.-W. Jin, Y.-C. Zou, K.-X. Xu, W.-X. Fang, L. Zhang and H. Dong, *Environ. Sci.: Nano*, 2021, **8**, 3665–3672.
- 36 J. Y. Wang, Y. H. Luo, F. H. Xing, X. W. Jin, L. H. Guo, L. H. Zhai, L. Zhang, W. X. Fang and B. W. Sun, *ACS Appl. Mater. Interfaces*, 2020, **12**, 15573–15578.
- 37 Y. H. Luo, M. Nihei, G. J. Wen, B. W. Sun and H. Oshio, *Inorg. Chem.*, 2016, **55**, 8147–8152.
- 38 Y.-H. Luo, Q.-L. Liu, L.-J. Yang, Y. Sun, J.-W. Wang, C.-Q. You and B.-W. Sun, *J. Mater. Chem. C*, 2016, **4**, 8061–8069.
- 39 Y. H. Luo, C. Chen, C. He, Y. Y. Zhu, D. L. Hong, X. T. He, P. J. An, H. S. Wu and B. W. Sun, *ACS Appl. Mater. Interfaces*, 2018, **10**, 28860–28867.
- 40 Y. H. Luo, X. T. He, C. Wang, J. Y. Wang, Z. Y. Zheng, J. Zhao, L. H. Guo, L. H. Zhai and B. W. Sun, *Mater. Today Nano*, 2020, **9**, 100068.
- 41 Y. H. Luo, S. H. Ma, H. Dong, Y. C. Zou, K. X. Xu, S. Su, X. W. Jin, L. Zhang and W. X. Fang, *Mater. Today Chem.*, 2021, **22**, 100517.
- 42 Y. H. Luo, L. Zhang, W. X. Fang, S. H. Ma, H. Dong, S. Su, Z. Y. Zheng, D. N. Li and L. H. Zhai, *Chem. Commun.*, 2021, **57**, 5901–5904.
- 43 Y. H. Luo, L. Zhang, H. Dong, S. H. Ma and F. L. Zeng, *Mater. Today Chem.*, 2022, **25**, 100923.
- 44 L. Zhang, W.-X. Fang, C. Wang, H. Dong, S.-H. Ma and Y.-H. Luo, *Inorg. Chem. Front.*, 2021, **8**, 898–913.